Sensitivity to Snapshot Frequency in the POD-based Reduced-Order Modeling of Flow over a Gaussian Bump

Donya Ramezanian[1], Michael W. Lee[2], Naili Xu[1†], and Iván Bermejo-Moreno[1‡]

[1]Department of Aerospace and Mechanical Engineering, University of Southern California
3650 McClintock Ave., Los Angeles, California, 90089, United State of America
dramezan@usc.edu; [†] nailixu@usc.edu; [‡] bermejom@usc.edu
[2]NASA Langley Research Center,
1 Nasa Dr, Hampton, Virginia, 23666, United States of America
michael.w.lee@nasa.gov

Abstract – The flow over a Gaussian bump at a Reynolds number of 10^6, based on the bump length and freestream conditions, and a Mach number of 0.2, was simulated using wall-modeled large eddy simulation (WMLES). The incoming turbulent flow exhibits relaminarization upstream of the bump apex, due to the favourable pressure gradient acceleration induced by the bump curvature, as well as separation, reattachment and a detached shear layer downstream of the apex. A Galerkin reduced-order model (ROM) was then constructed using a proper orthogonal decomposition (POD) modal basis. The complex, three-dimensional flow features are captured by spatial POD modes differently based on the frequency of the high-fidelity snapshots originally provided. POD modes constructed from differently sampled snapshot matrices were then truncated to retain 90% of the turbulence kinetic energy in the domain of interest. A parametric study is conducted to evaluate the effect of the frequency of snapshots used to construct the POD-ROM.

Keywords: POD, ROM, turbulent flow, relaminarization, separation

1. Introduction

Turbulent flows can be characterized by coherent structures, which play an important role in unravelling the underlying flow physics. Whether this enhanced understanding yields inexpensive, accurate simulations or insight into improved flow control, a common way to identify such structures is through empirical, linear bases. Owing to the broad range of spatiotemporal scales involved in turbulent flows, these linear bases must usually be constructed from costly datasets [1] obtained from experiments or high-fidelity simulations. The return on this investment can be a reduced-order model (ROM), which can provide a much more computationally inexpensive approach for the prediction of turbulent flows by retaining the most relevant coherent structures and their associated dynamics. For the price of one costly simulation, one can simulate several similar problems. A common challenge with this is ensuring that the ROMs are themselves reliable.

The Proper Orthogonal Decomposition (POD) is one of the most widely used modal decomposition techniques to analyze fluid flows. It does so by extracting modes optimized to span the mean square of the field variable of interest. This method was first introduced in the fluid dynamics and turbulence community by Ref. [2] but formerly had been proposed under a variety of names in other fields (see Ref. [3] and references therein). Performing the POD on velocity flow fields results in fluid structures that most contribute to the flow's kinetic energy. The nature of the optimization, and of the kinetic energy, means that larger-scale structures are more completely captured in an efficient manner; lower-energy structures may be dispersed among several higher modes. In addition to capturing the dominant features and coherent structures in flows, the POD has also been used extensively in the development of ROMs that represent the dynamics of the flow using the least number of modes with reasonable accuracy [4]. In many flow problems, especially involving turbulent flow, POD-ROMs based on Galerkin projection have yielded impressively accurate low-cost dynamical simulations of complicated flow regimes [5–7].

One determining factor in the performance and accuracy of a POD-ROM is the frequency of sampling. While applying a POD-ROM to datasets with insufficient frequency of sampling could result in missing influential flow physics, too frequent sampling results in unnecessary memory usage and computational costs. In the present work, we apply a POD-ROM approach for incompressible flow, following the development used in Ref. [8] to study a three-dimensional turbulent flow exhibiting relaminarization and separation. The objectives are to explore the effect of the frequency of snapshots in the performance of POD-ROM and evaluate how POD spatial modes capture relevant flow physics.

2. Methodology

We first conduct numerical wall-modeled large-eddy simulations (WMLES) of the fluid flow over a solid wall with a Gaussian bump shape given by $y/L = 0.085 \exp[-(x/0.195L)^2]$, where x and y are the horizontal and vertical coordinates, at a Reynolds number of 10^6 based on the bump length, L, the freestream density, ρ_∞, constant dynamic viscosity, μ, and freestream flow speed, U_∞. The WMLES computational domain, D, of extent $-0.98 < x/L < 2$, $0 < y/L < 0.45$, and $0 < z/L < 0.2$, where L is the bump length, is discretized by $1851 \times 66 \times 32$ hexahedral cells. The flow configuration follows that of Ref. [9]. An in-house, second-order finite-volume numerical solver of the LES-filtered compressible Navier-Stokes equations is used, with Vreman's subgrid-scale model [10] and an equilibrium wall-model [11]. Symmetry is imposed at the top boundary, periodicity in the spanwise direction, and synthetic turbulent flow at the inlet domain. The incoming turbulent flow relaminarizes in the favorable pressure gradient region upstream of the bump apex, transitions back to turbulence immediately downstream of the apex, separates in the adverse-pressure gradient, leeward side of the bump, and reattaches farther downstream. After the WMLES reaches a statistically stationary state, we store 1000 instantaneous, three-dimensional snapshots of the velocity field, equispaced a dimensionless time $\Delta t_s L/U_\infty = 1.53e - 5$, corresponding to 25 simulation time steps, for nondimensional simulation times between 37.898 and 38.278. The WMLES snapshots are the input data to the POD-ROM methodology considering three output frequencies of snapshots: a) every 25 time steps (1000 snapshots); b) every 50 time steps (500 snapshots); and c) every 100 time steps (250 snapshots).

Although a compressible flow solver is used in the WMLES, the low flow Mach number ($M_\infty = 0.2$) makes compressibility effects negligible. Thus, we formulate the POD-ROM methodology in terms of the incompressible Navier-Stokes equations (Einstein summation implied):

$$\partial_t u^i + u^j \partial_j u^i = -\partial_i P + Re^{-1}\partial_j^2 u^i \tag{1}$$

where u^i is the velocity component in the x_i spatial direction ($\boldsymbol{x} = \{x_i, i = 1,2,3\} \in D \subset \mathbb{R}^3$), P is the pressure, Re is the Reynolds number, ∂_t denotes the partial time derivative and ∂_j denotes the partial spatial derivative along the x_j coordinate direction. Subgrid scale terms resulting from the LES formalism and the wall-model boundary condition are not included explicitly in the POD-ROM formulation. Rather, closure of the governing equations is accomplished using the empirical modes themselves capturing all necessary spatial information. An inner product is defined in the spatial domain between two fields u^i and v^j as $\langle \boldsymbol{u}, \boldsymbol{v} \rangle = \int_D u^i v^j \, d\boldsymbol{x}$. The mean velocity field over all N_s snapshots is obtained from $\boldsymbol{u_0}(\boldsymbol{x}) = \sum_{n=1}^{N} \boldsymbol{u}(\boldsymbol{x}, t_n)/N_s$. Using a Galerkin decomposition of the velocity $u^i(\boldsymbol{x}, t) = u_0^i(\boldsymbol{x}) + u_f^i(\boldsymbol{x}, t)$, where $u_0^i(\boldsymbol{x})$ and $u_f^i(\boldsymbol{x}, t)$ represent the mean and fluctuating velocity fields, respectively, and substituting into Eq. (1) results in (see Ref. [8]):

$$\partial_t u_f^i = -\partial_t u_0^i - u_0^j \partial_j u_0^i - u_0^j \partial_j u_f^i - u_f^j \partial_j u_0^i - u_f^j \partial_j u_f^i - \partial_i P + Re^{-1}(\partial_j^2 u_0^i + \partial_j^2 u_f^i) \tag{2}$$

All three snapshot matrices are full rank. Applying a singular-value decomposition (SVD) of the matrix of fluctuating velocity snapshots (obtained by subtracting the mean velocity from each original velocity field snapshot), we can express $u_f^i(\boldsymbol{x}, t)$ as a weighted expansion $u_f^i(\boldsymbol{x}, t) \approx \sum_{n=1}^{r} a_n(t)\phi_n^i(\boldsymbol{x})$, where $a_n(t)$ and $\phi_n^i(\boldsymbol{x})$ are the nth temporal coefficient and spatial mode, respectively, with $r \leq N$ being the number of retained modes. The resulting POD modes are orthonormal. The SVD's eigenvalues represent the mean kinetic energy in the corresponding modes. The POD modes are sorted by largest eigenvalue, which equates to the mode's mean kinetic energy content. Substituting the modal decomposition in Eq. (2) and taking a weighted integral where the weighting function is the kth velocity mode results in a system of r temporal differential equations for the modal coefficients [8]:

$$\dot{\boldsymbol{a}} = \boldsymbol{a}^T \boldsymbol{Q}\boldsymbol{a} + (\boldsymbol{L}^0 + Re^{-1}\boldsymbol{L}^{Re})\boldsymbol{a} + \boldsymbol{P} + \boldsymbol{C}^0 + Re^{-1}\boldsymbol{C}^{Re} \tag{3}$$

where $Q_{knm} = -\langle \phi_k^i, \phi_m^j \partial_j \phi_n^i \rangle$, $L_{kn}^0 = -\langle \phi_k^i, u_0^j \partial_j \phi_n^i + \phi_n^j \partial_j u_0^i \rangle$, $L_{kn}^{Re} = \langle \phi_k^i, \partial_j^2 \phi_n^i \rangle$, $p_k = \langle \phi_k^i, \partial_i P \rangle$, $c_k^0 = -\langle \phi_k^i, u_0^j \partial_j u_0^i \rangle$, $c_k^{Re} = \langle \phi_k^i, \partial_j^2 u_0^i \rangle$. The contribution from the pressure term, $\boldsymbol{P}$, which is zero for incompressible flows if all modes satisfy homogeneous Dirichlet boundary conditions [8], is assumed to be negligible in this work. First- and second-order derivative terms contributing to terms in Eq. 3 are calculated by 6th-order accurate finite difference schemes. The number of modes r preserved in all the cases retains 90% of total kinetic energy.

3. Results

Fig. 1a shows the logarithmic normalized eigenvalue trend from each data set and the number of modes required to preserve 90% of energy, corresponding respectively to 173, 169, and 154 modes for snapshot frequencies of 25, 50, and 100 time steps. Figure 1b shows the temporal evolution of error of the reconstructed velocity field attained from POD-ROM solutions for the three study cases, defined as $\text{err}(t) = \sum_{k=1}^{N_c} \text{w}(k) [u_{\text{WMLES}}^i(k, t) - u_{\text{ROM}}^i(k, t)]^2$, where N_c is number of

cells in the domain of interest, w is the kth cell volume, u_{WMLES}^i is the reference velocity solution and u_{ROM}^i is the reconstructed POD-ROM velocity. The frequency of snapshots is observed to affect the accuracy of the POD-ROM solution in short time, while in long time the POD-ROM performs more similarly for the three cases. This convergent error is observed to increase gradually in magnitude (readers should note the logarithmic scale on Fig. 1b) over the course of the simulation, though the trend is not dramatic enough to indicate whether the POD-ROM solutions would be stable in very long time. Rather, this indicates that despite the differences in instantaneous dynamics, the three bases yield simulations with comparable global stability and accuracy.
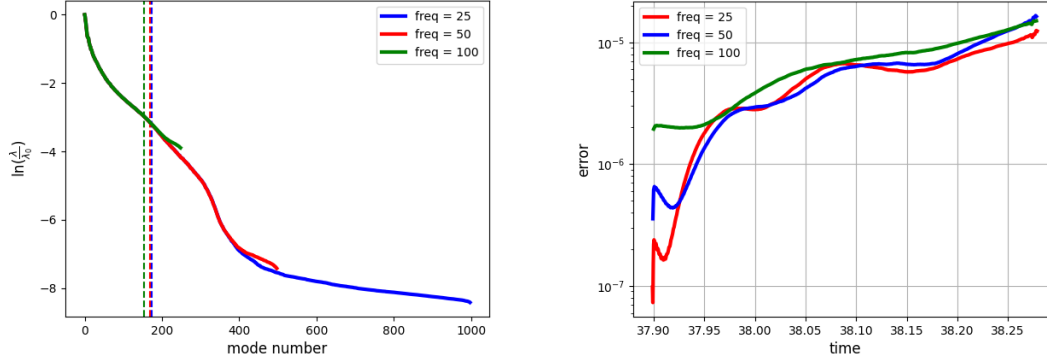
Fig. 1: (a) Logarithmic trend in normalized POD eigenvalues based on snapshots of the WMLES velocity field at three different sampling frequencies (every 25, 50, 100 time steps). The dashed lines represent the number of modes required to preserve 90% of total energy for each case. (b) Temporal evolution of error of reconstructed POD-ROM velocity field compared with WMLES data.

Figure 2 compares three modal coefficients over time, obtained from the POD and POD-ROM integration, for different snapshot frequencies. The higher-energy a_{ROM} and a_{POD} coefficients (those with larger eigenvalues) agree more closely, while for less dominant modes the mode-normalized deviations are more significant. Representative spatial modes of the velocity are shown in Fig. 3, highlighting the corresponding flow structures (shape and scales) near the Gaussian bump and in the relaminarization (upstream of the apex) and separated (downstream) regions.
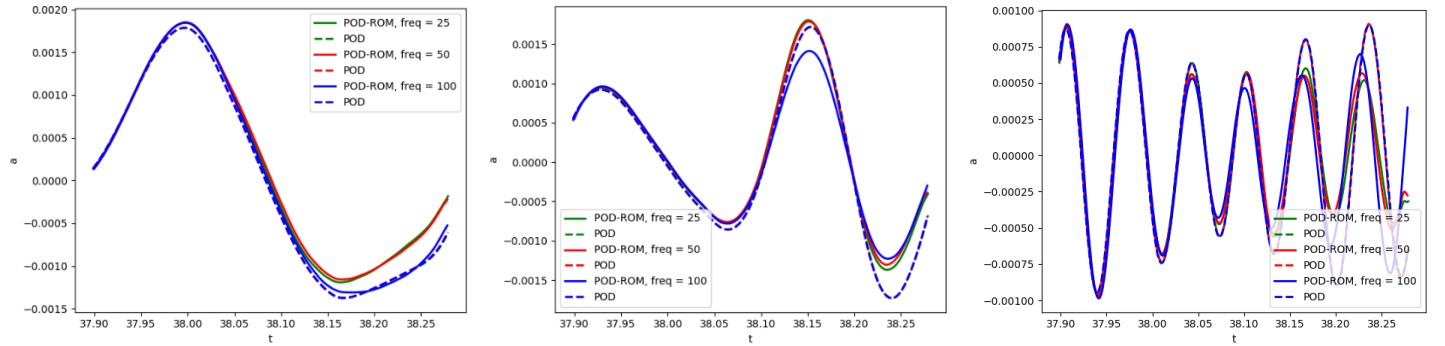

Fig. 2: Comparison of modal coefficients over time corresponding to different mode numbers obtained from POD-ROM and POD at different snapshot frequencies: mode numbers 1 (left), 2 (center), and 10 (right).
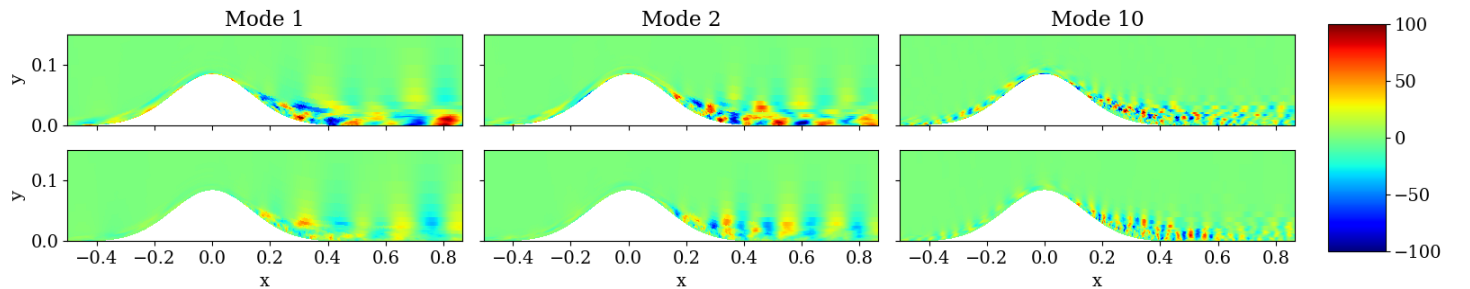

Fig. 3: Contours on a vertical (xy) plane of the first, second, and tenth spatial POD modes for the horizontal (top row) and vertical (bottom row) velocity components, obtained from snapshots extracted every 25 time steps, focused near the Gaussian bump.

It is clear from these plots that the more coherent, energy-containing flow structures are less sensitive to the sampling frequency of the snapshot matrix, which may indicate that these earlier modes are dominated by lower frequencies that are still captured even when the frequency of flow snapshots is reduced. However, an interpretation more consistent with the mathematics of the POD is that these modes are simply more coherent regardless of sampling frequency because the more significant energy-containing structures are what the POD primarily optimizes for. The less energetically important – but still dynamically critical – higher modes fluctuate in structure due to even minor changes in the snapshot matrix, although the overall system physics are still captured similarly by the different modal bases.

4. Conclusions

Application of POD to velocity datasets obtained from wall-modeled LES of the nearly-incompressible flow over a Gaussian bump exhibiting relaminarization and separation in the statistically stationary regime shows that the most energetic spatial modes are able to capture the flow features corresponding to the shear layer produced by the boundary layer detachment, whereas the less dominant (higher-order) modes encompass the finer turbulent scales, some of which are dampened in the relaminarization region upstream of the bump. A parametric study conducted by considering POD-ROM reconstructions from datasets obtained at three different frequencies of snapshots output from the WMLES shows a more noticeable effect of the frequency in the higher-order modes, with the largest discrepancies in the error of the POD-ROM reconstructed velocity appearing at early integration times. Differences based on the temporal resolution of the input data decrease at later times, indicating that the accumulated error from the spatial reconstruction and the ROM integration may become dominant for the flow, frequencies, and modelling assumptions considered in the present study.

References

[1] Kostas, J., Soria, J., and Chong, M. S., "A comparison between snapshot POD analysis of PIV velocity and vorticity data," Exp. Fluids, Vol. 38, No. 2, 2005, pp. 146–160.

[2] Berkooz, G., Holmes, P., and Lumley, J. L., "The proper orthogonal decomposition in the analysis of turbulent flows," Ann. Rev. Fluid Mech. Vol. 25, No. 1, 1993, pp. 539–575.

[3] Taira, Kunihiko, et al. "Modal analysis of fluid flows: An overview." AIAA J. 55.12 (2017): 4013-4041.

[4] Delville, J., Ukeiley, L., Cordier, L., Bonnet, J.-P., and Glauser, M., "Examination of large-scale structures in a turbulent plane mixing layer. Part 1. Proper orthogonal decomposition," Journal of Fluid Mechanics, Vol. 391, 1999, pp. 91–122.

[5] Arndt, R. E., Long, D., and Glauser, M., "The proper orthogonal decomposition of pressure fluctuations surrounding a turbulent jet," J. Fluid Mech., Vol. 340, 1997, pp. 1–33.

[6] Weller, J., Lombardi, E., Bergmann, M., and Iollo, A., "Numerical methods for low-order modeling of fluid flows based on POD," Int. J. Numer. Methods Fluids, Vol. 63, No. 2, 2010, pp. 249–268.

[7] Balajewicz, M. J., Dowell, E. H., and Noack, B. R., "Low-dimensional modelling of high-Reynolds-number shear flows incorporating constraints from the Navier–Stokes equation," J. Fluid Mech., Vol. 729, 2013, pp. 285–308.

[8] Lee, M. W., and Dowell, E. H., "On the Importance of Numerical Error in Constructing POD-based Reduced-Order Models of Nonlinear Fluid Flows," AIAA Scitech 2020 Forum, 2020, p. 1067.

[9] Uzun, A., and Malik, M. R., "Simulation of a turbulent flow subjected to favorable and adverse pressure gradients," Theor. Comput. Fluid Dyn., Vol. 35, No. 3, 2021, pp. 293–329.

[10] Vreman, A. W., "An eddy-viscosity subgrid-scale model for turbulent shear flow: Algebraic theory and applications," Phys. Fluids, Vol. 16, No. 10, 2004, pp. 3670–3681.

[11] Kawai, S., and Larsson, J., "Wall-modeling in large eddy simulation: length scales, grid resolution and accuracy," Phys. Fluids, Vol. 24, 2012, p. 015105.